Astron. Astrophys. 347, 676–683 (1999)

ASTRONOMY AND ASTROPHYSICS

Proton and hydrogen temperatures at the base of the solar polar corona

E. Marsch[1], **C.-Y. Tu**[1,2], **P. Heinzel**[3], **K. Wilhelm**[1], **and W. Curdt**[1]

[1] Max-Planck-Institut für Aeronomie, D-37191 Katlenburg-Lindau, Germany
[2] Department of Geophysics, Peking University, Beijing, 100871, P.R. China
[3] Astronomical Institute, Academy of Sciences of the Czech Republic, CZ-25165 Ondřejov, Czech Republic

Received 11 February 1999 / Accepted 19 May 1999

Abstract. The SUMER (Solar Ultraviolet Measurements of Emitted Radiation) Spectrometer on SOHO (Solar and Heliospheric Observatory) has been used to observe the lines of the Lyman series (up to quantum numbers larger than 20) of hydrogen emitted in the solar atmosphere. The line shapes and intensities versus height are obtained near the limb from about -10″ to 70″. The lines are broad and show the typical self-absorption reversal near the limb, where the emission comes from optically thick material, and change systematically with increasing height. The H I Ly6, Ly7 and Ly9 lines attain a Gaussian shape at heights above the visible limb between about 19″ and 22″, where the emission comes from an optically thin plasma. The line shapes and intensities can be fitted well by model profiles obtained from multilevel NLTE (Non Local-Thermodynamic-Equilibrium) radiative transfer calculations which allow us, assuming excitation and ionization equilibrium, to derive consistently the temperatures and densities of the hydrogen atoms and, with additional assumptions, of the protons. Temperature values range between 1 10^5 K to 2 10^5 K. We present the systematics of the line shapes as observed in different emission regions and discuss briefly the relevance of these results for the solar wind acceleration and coronal heating.

Key words: line: profiles – Sun: corona – Sun: UV radiation

1. Introduction

The ESA's and NASA's Solar and Heliospheric Observatory (SOHO) was launched in December 1995 with one of the main goals to investigate the heating of the corona and the acceleration of the solar wind. In order to make progress in our understanding, better and specific knowledge of the coronal boundary conditions for the solar wind and of the plasma state in the transition region of the polar coronal holes is needed. Recent spectroscopic observations from SOHO clearly indicate substantial deviations of the plasma from local thermodynamic or collisional equilibrium. This conclusion comes from measurements of EUV emission lines as obtained on SOHO from the SUMER (Solar Ultraviolet Measurements of Emitted Radiation), CDS (Coronal Diagnostics Spectrometer) and UVCS (Ultraviolet Coronagraph Spectrometer) instruments, which show that heavy ions, coming in various ionization stages in the corona, are rather hot (Hassler et al., 1997; Seely et al., 1997; Marsch et al., 1997; Kohl et al., 1997, 1998), particularly in the polar coronal holes, whereas the electrons are relatively cold (David et al., 1998; Wilhelm et al., 1998a). The ions show some ordering of their kinetic temperatures according to the local gyrofrequencies (Tu et al., 1998; Cranmer et al., 1999a), a result which might indicate that cyclotron-resonant wave-particle processes are being responsible for the coronal heating. Also, flow speeds in the low corona (Peter, 1999; Hassler et al., 1999; Dammasch et al., 1999; Peter & Judge, 1999) and the high corona (Kohl et al., 1997; Cranmer et al., 1999b) have recently been determined for the first time with SOHO.

What is still missing in the literature are the temperatures, T_p and T_α, of the major ion species, protons and α particles, which do of course not emit any light and thus cannot be diagnosed directly by spectroscopic means. UVCS observes routinely the H I Lyman α line, the shape of which allows one to derive T_p profiles out to a few solar radii ($R_\odot$). The proton temperatures can be inferred under the assumption that due to charge exchange the ions and neutrals are still coupled strongly enough so that their kinetic temperatures are equal (Kohl et al., 1997). Similarly, the higher members of the H I Lyman series observed by SUMER (Wilhelm et al., 1997a) can be used to obtain the temperature of hydrogen, and thus T_p at the bottom of the corona, defined here to be at about 20″ ($\approx$ 14300 km; 1″at SOHO is equivalent to $\approx$ 715 km at the Sun) above the visible limb. However, the data can only be interpreted correctly if multilevel NLTE (Non Local-Thermodynamic-Equilibrium) radiative transfer calculations (Heinzel, 1995) are employed to explain the measured line shapes within such model results. This paper presents the first estimates of the proton temperature in the low polar corona and thus provides fundamental data on the coronal plasma state and important boundary values for models of the fast solar wind.

2. Observations and data reduction

The SUMER spectrometer, its in-flight performance and first results have been described elsewhere (Wilhelm et al., 1995, 1997a; Lemaire et al., 1997). SUMER is a stigmatic normal-

Send offprint requests to: E. Marsch (marsch@linmpi.mpg.de)

Table 1. Description of data sets

Data set	Observation Date	Slit size	Centre of slit (Sun x, Sun y)	Exposure time × number of images	Spectral range (pixels; Å)
1	1998 Nov 7	$1'' \times 120''$	$(0'', 1020'')$	(115 s)×161	1024; 46
2	1996 Dec 11	$1'' \times 300''$	$(0'', 983'')$	(30 s)×337	25; 1

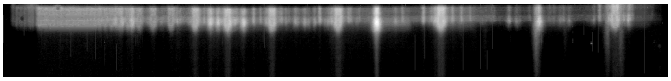

Fig. 1. Raw image of the SUMER $1'' \times 120''$ slit dispersed in wavelength over the range from 910 Å to 951 Å, covering the hydrogen Lyman series beyond Ly4 and the recombination continuum (diffuse band on the left). The solar limb is approximately coincident with the sharp edge between the background continuum and the dark void. The data refer to set 1.

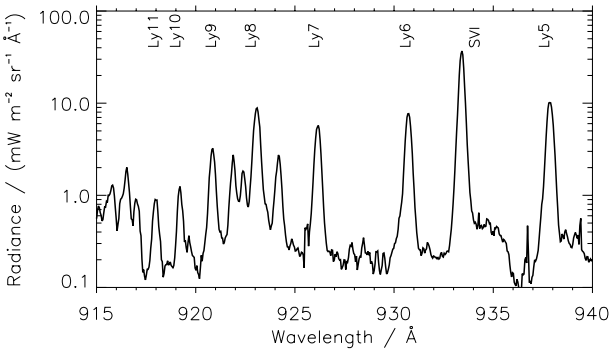

Fig. 2. SUMER spectrum from 915 Å to 940 Å, including the Lyman series from Ly5 to Ly11 and beyond. Note that Ly11 is on the bare part of detector B. We did not correct this, and thus the Ly11 intensity may not be reliable. The spectrum is obtained from data set 1 by averaging over the height range from $19''$ to $22''$.

incidence and high-resolution spectrometer which covers the spectral range between about 400 Å and 1600 Å, has spectral pixel sizes of 42–45 mÅ and can thus measure the entire H I Lyman series plus the hydrogen recombination continuum. SUMER resolves the individual lines of the series up to high quantum numbers, depending on the observed structure. For representative examples, see the recent papers by Warren et al. (1998) and Curdt and Heinzel (1998) with observations of the quiet-Sun structure on the solar disk. We have searched the whole SUMER archive for data appropiate for a study of the H I Lyman series measured at and off the limb in a polar coronal hole. Only very few observational periods were found to be useful for this purpose, and therefore we recently carried out an additional observational sequence of the Lyman series. The data used in this paper are from two observation periods. The corresponding parameters are listed in Table 1.

For the data set 2 we used the $1'' \times 300''$ slit and detector B, by which the spectra were acquired on 300 spatial × 25 spectral pixels, corresponding to a window positioned around the Ly6 line. For the data set 1 we used the $1'' \times 120''$ slit and also detector B, by which the spectra were acquired on its central band of 120 spatial × 1024 spectral pixels, which covered the spectral range from 910 Å to 951 Å (attenuators excluded) thus avoiding the strongest Lyman lines. One raw image on the detector is illustrated in Fig. 1. The solar limb is visible as a sharp edge and by the drop of the intensity of the background continuum, from which the Lyman lines can clearly be discerned as the bright stripes that extend over the limb and then gradually fade away as thin spikes. The Lyman lines are seen lower in the atmosphere in direct emission and then with increasing height above the solar limb as scattered light. There are many other lines in the spectrum which yet are not of interest for this study.

To obtain the raw spectrum as shown in Fig. 1 the data has been first decompressed and then flat-field corrected. The geometrical distortion of the detector was corrected by the standard destretching procedure of the SUMER software, which also compensates for the small slit-image inclination with respect to the pixel orientation. The spectral pixels were then transformed into wavelengths by calibration routines (Wilhelm et al., 1997a), and finally the measured intensity (in counts) of the lines was converted into radiometrically calibrated spectral radiances (Wilhelm et al., 1997b, 1998b). An example of the resulting spectrum, which is obtained by averaging over the height range from $19''$ to $22''$, is shown in Fig. 2. The coordinate origin, $0''$, corresponds to the position of the visible limb, which is about $3''$ below the position of the maximum of the Ly6 radiance profile as shown in the subsequent Fig. 5. In order to determine the position of the visible limb with respect to the maximum limb brightenings of the Lyman lines, a comparison of the lines Ly6, Ly7 and Ly9 with images from the SUMER Rear Slit Camera (RSC) was recently (on March 19, 1999) made near the north polar limb of the Sun. We found the Lyman-line maxima at locations between $1''.5$ and $3''$ above the visible limb. Similarly, the continuum between 927 Å and 929 Å, or the maximum of a neighbouring line such as O I (λ936), was found to peak at about $3''$ above the visible limb. These observational result are consistent with a determination of the relative limb position using, e.g., the C I continuum formed on the chromospheric plateau between $2''$ and $3''$ (Vernazza et al., 1973; Vernazza et al., 1981).

The Fig. 2 gives the Lyman series, including, e.g., Ly5 ($\lambda 937.803$) or Ly6 ($\lambda 930.748$) on the right hand side with a strong line of S VI in between. (The shoulder on the red side of S VI at about 1% of the peak intensity is a detector artefact. It does not, however, affect the lines discussed in this communication). The data of Fig. 2 indicate that the line shapes of all lines from Ly6 to Ly10 are Gaussian, with the exception of Ly5 which appears somewhat saturated.

All Lyman lines investigated here are blended to some extent (cf., Wilhelm et al., 1997a; Curdt et al., 1997a), e.g., by lines of the He II Balmer series. We have selected members of the hydrogen Lyman series where we know the contribution of blends to be less than 10% and thus do not expect a visible influence on line profiles or broadenings. The Ly6 line is blended by the He II Ba12 ($\lambda 930.34$) line and O I ($\lambda\lambda 930.256, 930.886$) lines. The blend in the blue wing can partly be resolved, its contribution is ouside the line profile of interest. The blend in the red wing is very close to the laboratory wavelength and obviously not strong enough to affect the full width at half maximum (FWHM). The Ly7 is blended by the He II Ba14 ($\lambda 925.82$) line, for which the same argument applies as in the case of Ly6, and by a line at $\lambda = 926.3$ Å, which was identified as the O I ($\lambda 926.295$) line by Curdt et al. (1997a). However, from Fig. 7 we conclude that plasma at a higher temperature is more likely the emitting source. This blend certainly increases the FWHM. The effect is assumed to be less than a quarter of a pixel (11 mA). The Ly9 line is blended by the He II Ba18 ($\lambda 920.56$) line in the blue wing, which again can be partly resolved. All these blends are not serious and do not compromise our analysis and subsequent conclusions.

From such spectra as shown in Fig. 1 one can deduce height profiles of any particular line (for example, for Ly6, falling into a narrow spectral window with a size of 30 spectral pixels) and thus obtain the profiles of the intensity and line shape with altitude. It turned out that the Lyman lines are still visible beyond about 30″, but there they represent only stray light from intense emissions on the disk and at the limb. In order to get good statistics and smooth spectral profiles, the data have been averaged over four spatial pixels and over many exposures (see Table 1). In calculating the variation of the intensity with height, we added the spectral intensities of all pixels in the corresponding window of a line and obtained the integrated line radiance in units of W m $^{-2}$ sr^{-1}. Since only the intensity and shape of a line are of interest in this work, we did not try to identify possible Doppler shifts of the lines considered. The wavelengths given in Fig. 2 are determined by the image parameters, i.e., by the reference wavelength and instrumental dispersion. In the following figures showing individual line profiles we assumed the wavelengths at the peak intensity to coincide with the wavelengths as identified by Curdt & Heinzel (1998) in their on-disk observations of the Lyman series.

3. Observational results and analysis

We have obtained several time series with observations of the Lyman lines on and off the solar limb, only two of which we show here in more detail. The Table 1 summarizes the instrument settings for these observations and other relevant parameters. Intensities in what follows are given in absolute units (for the SUMER radiometric calibration see Wilhelm et al., 1997b, 1998b) in order to be able to compare subsequently with NLTE model calculations.

In Fig. 3 the radiance of the H I Ly6 ($\lambda 930.748$) line is plotted versus relative height in arcseconds. Note that the intensity

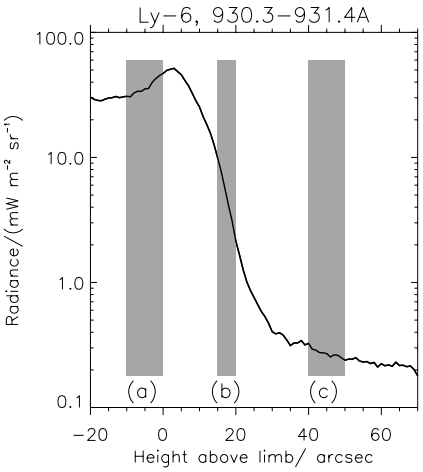

Fig. 3. Radiance of the H I Ly6 line (integrated intensity; data set 2) versus height over the solar limb in arcseconds. The data correspond to a period near solar minimum and were obtained in a polar coronal hole. The gray-shaded bars (a), (b), (c) indicate the altitude intervals (from $-10''$ to $0''$, $15''$ to $20''$, and $40''$ to $50''$), over which the data were averaged in order to obtain the line profiles dispayed in Fig. 4. Note the steep intensity decline with height.

increases from the disk to a maximum value off limb, which is located near 3″ and is equal to about twice the disk value. This is expected for a line of sight (LOS) tangent to the limb for an optically thin medium, in which case the plasma column simply doubles in length. The three shaded bars indicate the distance range over which the data were averaged to obtain the typical line profiles shown in Fig. 4, which give the spectral radiance versus wavelengths. The intensity of Ly6 steeply decreases with altitude up to 30″ and then levels off more slowly. This last part of the curve corresponds to stray light stemming from Ly6 emission on the disk and at the limb.

The characteristic changes of the line profile with height are illustrated in Fig. 4. The top profile (a) reveals the distinct signature of self-absorption of the Ly6 line emerging from an optically thick plasma column. The middle profile (b) shows a Gaussian shape. The bottom profile (c) stems from scattered light and has very low intensity, but reflects the same typical dip in the centre of the line as the top profile. Several other observational periods (not shown here) yielded qualitatively similar results. Before we continue, some discussion on the scattered light contribution to the profile (b), which is taken in the strong radiance gradient off the limb, is required to evaluate and retrieve the real coronal contribution to the emission. We have used the radial straylight profile of the O I ($\lambda 936$) line to estimate the scattered light level. It is about 3% at 14″, 2% at 23″, 1% at 38″ and 0.5% at 50″. Similar levels can be assumed for the Lyman lines. Given the intensity of the profile (a) at the top in Fig. 4, one can expect an overall scattered-light contribution of at most 10% to the profile (b), which has no serious influence on the subsequent results and conclusions. Consequently, we did not subtract a scattered-light contribution from all the (b)-profiles discussed below. Profile (c) can be fully explained

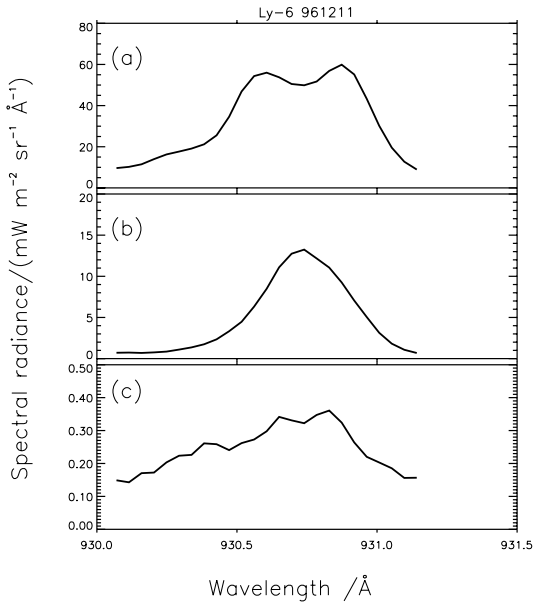

Fig. 4a–c. Profiles of the spectral radiance of the H I Lyman Ly6 line for the three reference heights **a**, **b**, **c** shown in Fig. 3. Note the change in the line shape with height. The data refer to data set 2.

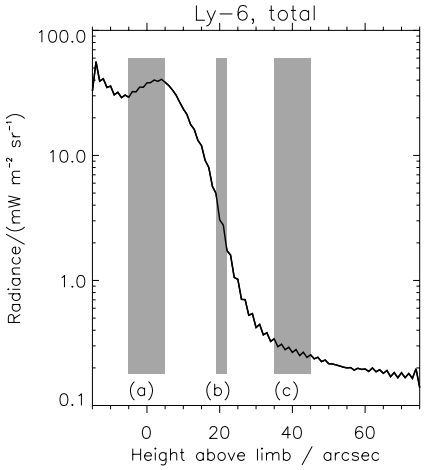

Fig. 5. Radiance of the H I Ly6 line versus height over the solar limb in arcseconds. The data correspond to a period of increasing solar activity and were obtained in a northern polar coronal hole (data set 1). The gray-shaded bars (a), (b), (c) indicate the altitude intervals (from $-5''$ to $10''$, $19''$ to $22''$, and $35''$ to $45''$), over which the data were averaged in order to obtain the line profiles dispayed in Fig. 4. Note the steep intensity decline with height.

as being due to scattered light at a 0.5% to 1% level of profile (a).

The Ly6 emission coming from the layer (b) in Fig. 4 between $15''$ and $20''$ is consistently explained as originating from optically thin material, since the line is Gaussian down to a one-percent level. The line width, expressed in terms of the standard deviation of the Gauss fit, is 3.25 spectral pixels. One pixel at this wavelength corresponds to 44.7 mÅ. The instrumental line broadening of SUMER has been measured. Standard software is available for quantitative correction. The effect on the observed Lyman lines is 22 mA. Also, thermoelastic effects of the temperature control of the spectrometer (Curdt et al., 1997b) and residual errors of the geometrical correction procedure may contribute to instrumental line broadening to some extent, although this is certainly a minor effect. After correction for the instrumental line broadening, the FWHM of the Ly6 line (data set 2) is 323.1 mÅ. The measured FWHM of a line can be converted into an effective Doppler speed by means of the usual formula:

$$V_{eff} = 0.6006 \text{ FWHM } \frac{c}{\lambda} \tag{1}$$

with the speed of light, c, and the wavelength, λ, under consideration. The line broadening may consist of two distinct contributions, stemming from thermal motions and small-scale unresolved wave or turbulent motions. If the corresponding velocity distributions are both assumed to be Gaussian, we can superpose these distributions and simply add their variances to produce an effective speed

$$V_{eff}^2 = \frac{2k_B T_{eff}}{m_H} = \frac{2k_B T_H}{m_H} + \xi^2 \tag{2}$$

Here T_{eff} is the effective temperature defined through the Doppler speed, T_H is the kinetic temperature of hydrogen atoms in the line of sight, m_H is their mass, k_B is Boltzmann's constant, and $\xi^2 = 2/d < \delta v^2 >$ the turbulent speed, where $< \delta v^2 >$ is the standard deviation of the velocity distribution of the turbulence in the LOS, and d is the dimension of the turbulent fluctuations, e.g., 2 for an Alfvén wave. With Eqs. (1) and (2) we obtain the values: $V_{eff} = 62.4$ km s^{-1} and $T_{eff} = 2.4\ 10^5$ K. If we assume $\xi = 30$ km s^{-1}, a parameter corresponding to the maximum turbulent broadening of heavy ion lines emitted around 10^5 K (e.g., Mariska, 1992; Brekke et al., 1997; Chae et al., 1998) we obtain $T_H = 1.8\ 10^5$ K. Of course, the line intensity profile cannot be interpreted so simply but requires radiative-transfer modelling as discussed below.

In Fig. 5 the radiance of the H I Ly6 ($\lambda 930.748$) line is plotted again versus relative height in arcseconds, but now for a data set which was obtained in a polar coronal hole observed during the phase of the solar cycle when the Sun's activity increased (see Table 1 for the dates). Generally, Fig. 5 is similar to Fig. 3, but the radiance profile is more noisy. One reason for this behaviour is that the location of the photosensitive area of the detector is not absolutely stable with time, which has the effect that signatures of the photocathode are observed with a shift of up to one pixel. This long-term drift has an effect on the quality of the flat-field correction as described by Carlsson et al. (1997). This instrumental effect is not relevant for our analysis, but can still be seen as odd-even pattern in the radiance fall-off curve of Fig. 5, although the curve has been obtained through smoothing of the original profile by taking 5-point gliding averages. The height profile of the Ly6 radiance during this period looks qualitatively similar to the one of Fig. 5 at heights above $-5''$, with the exception of the first ten spatial pixels, and also reveals the rapid decline of the intensity with height down to levels where stray light prevails. The corresponding line pro-

Table 2. Line widths, temperatures and formation heights of the Gaussian-shaped Lyman lines (data set 1)

Ly	λ (Å)	FWHM (mÅ)	T_{eff} (10^5 K)	V_{eff} (km s^{-1})	$T_H(\xi = 30$ km s$^{-1})$ (10^5 K)	Height range
5	937.80	322.7	2.3	62	1.8	$22'' - 25''$
6	930.75	277.9	1.8	54	1.2	$19'' - 22''$
7	926.23	286.0	1.9	56	1.3	$19'' - 22''$
9	920.96	254.6	1.5	50	1.0	$19'' - 22''$
11	918.13	249.5	1.5	49	0.9	$15'' - 18''$

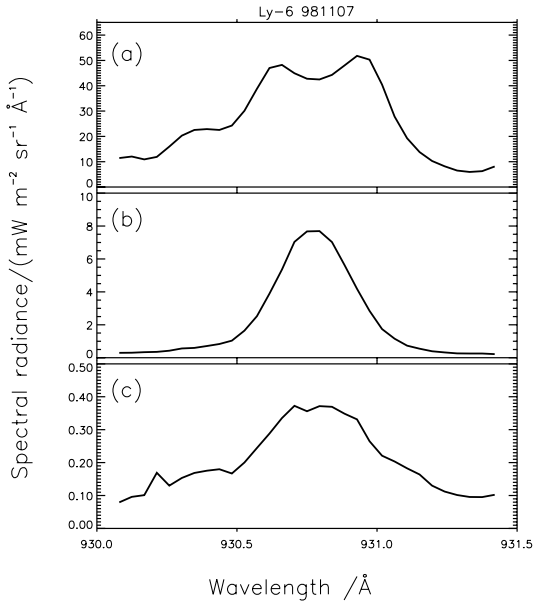

Fig. 6a–c. Line profiles of the spectral radiance of the Lyman Ly6 line for the three height intervals **a**, **b**, **c** shown in Fig. 5 as shaded bars. Note the changes in the apparent shape with height. The data refer to data set 1.

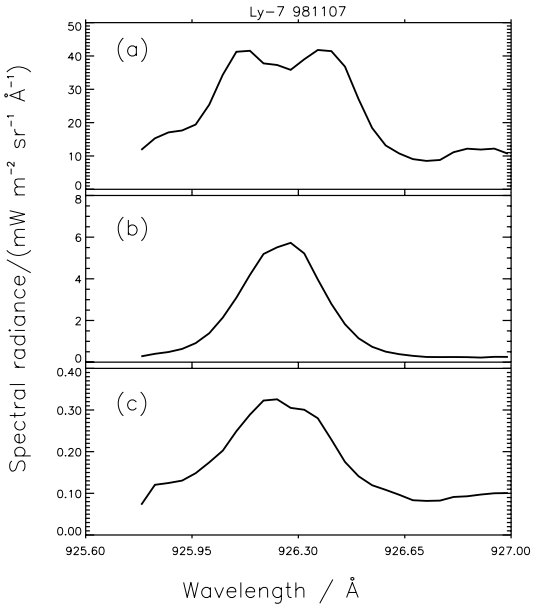

Fig. 7a–c. Line profiles of the spectral radiance of the Lyman Ly7 line for the same three reference heights **a**, **b**, **c** shown in Fig. 5. Note the changes in the apparent shape with height. The data correspond to a period of increasing solar activity and were obtained in a northern polar coronal hole (data set 1).

files of Ly6 obtained at three characteristic heights are shown in Fig. 6.

A transition from a double-humped profile with a self-absorption reversal to a Gaussian and then back to a broad and slightly indented profile is visible. This transition is actually gradual if a sequence of profiles is considered, while proceeding in arcsecond steps. But only a few of all profiles observed between $15''$ and $22''$ exhibit a clear Gaussian shape. The details are listed in Table 2, which gives, in the last column, the individual height range where each line appears Gaussian. Note, that the location of the corresponding interval tends to move to lower heights with increasing serial number of the lines. At lower heights, the LOS intersects a larger portion of the corona, which is optically thin only for the higher Lyman lines. Therefore, they still exhibit Gaussian profiles. Two examples of the higher-order lines are provided in Figs. 7 and 8, showing profiles of Ly7 and Ly9.

If we interpret the Gaussian-shaped Lyman lines shown in the respective middle panels of Figs. 4, 6, 7, and 8 as optically thin emission of the hot coronal plasma and use again Eq. (2), we can derive either a hydrogen effective temperature or a kinetic temperature and turbulence amplitude, as was already done for the Ly6 line above. The results are compiled in Table 2.

Typical uncertainties of the temperatures and speeds are 10 to 20%. The kinetic temperature, T_H, has been calculated with an assumed turbulent speed of $\xi = 30$ km s^{-1}. The line width described by the FWHM decreases systematically for all five lines (except Ly7, which is probably an effect of the unidentified line blend discussed in Sect. 2) from about 323 mÅ to 250 mÅ, corresponding to an effective temperature of 1.5 to 2.3 10^5 K, or about 1 to 2 10^5 K for a turbulent speed of $\xi = 30$ km s^{-1}, which is, at that formation temperature, the maximum value inferred from EUV emission lines of heavy ions in the transition region and lower corona after Mariska (1992) and Chae et al. (1998). The line width in terms of FWHM and the effective and kinetic temperatures decrease systematically with increasing serial number of the line. Otherwise, the behaviour of all Lyman lines is qualitatively similar, although substantial differences exist in their radiances.

Since the charge exchange rates between H I and protons are fast (time scales of seconds; see Olsen et al., 1994), the minority

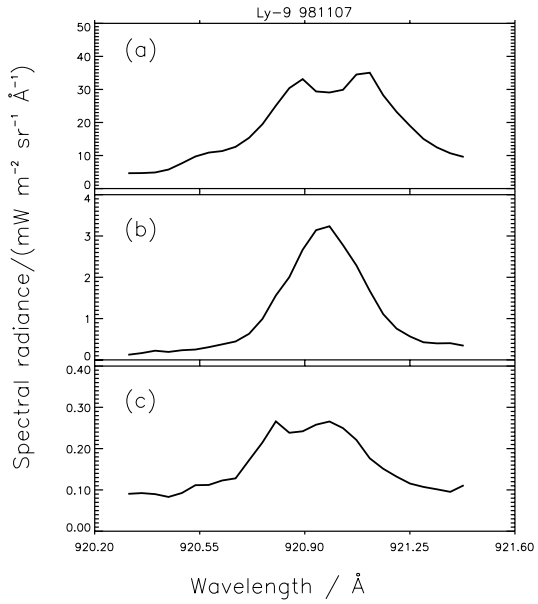

Fig. 8a–c. Line profiles of the spectral radiance of the Lyman Ly9 line for the same three reference heights **a**, **b**, **c** shown in Fig. 5. Note the changes in the apparent shape with height. The data correspond to a period of increasing solar activity and were obtained in a northern polar coronal hole (data set 1).

species H I can be expected to have the same temperature as the protons, and thus Table 2 may be considered as relating equally well to protons. The associated altitude is $20''$, which gives a height above the visible limb of about 14300 km. This height we define here as the bottom of the corona, where the network field in the form of funnels have typically been expanded and formed the more homogeneous coronal hole magnetic field. See, e.g, the network model of Gabriel (1976) or the recent funnel model of Hackenberg et al. (1999). High-resolution Sac Peak observations of spicules in Hα (Koutchmy, private communication) show their thin filamentary nature and short radial extension, hardly exceeding $10''$ above the visible limb (Roberts, 1945). Impulsive events observed in polar coronal holes (Koutchmy & Loucif, 1991) may reach higher but are rare. Consequently, there seems to be no danger that our Lyman lines, as shown in panels (b) of Figs. 6, 7, and 8, are contaminated by cool plasma emission. They represent genuine coronal material.

4. Model calculations

As the following theoretical considerations will show, the observed emission line shapes and calibrated intensities can be fitted well by model profiles obtained from multilevel NLTE-radiative-transfer calculations which allow us to estimate the range of temperatures, turbulent velocities, densities and geometrical extensions. While a Gaussian line profile gives us directly the value of a mean Doppler width (for optically-thin plasma integrated along the LOS), the (calibrated) line intensities have to be interpreted by means of rather complex modelling needed for plasmas which are not in thermal equilibrium (or LTE).

Here we consider a plasma volume at temperatures derived in Table 2, located above the solar surface at heights also given in Table 2, namely we take the range $19'' - 22''$ for the lines Ly6, Ly7 and Ly9, which corresponds to a mean height of about 14700 km above the limb. This plasma volume is supposed to be isothermal and to have a uniform electron density. We have not taken the radial density variation along the tangential LOS into account. The equivalent geometrical extension, d_M, of the uniform plasma column along the LOS is a free model parameter. We do not consider here the fine structure of this volume, i.e., individual vertical polar plumes and inter-plume lanes, because the plasma is optically thin in all considered transitions, and we can integrate its emission along the LOS. Finally, our model structure is static and assumed to be irradiated by the solar-disk intensity like in the case of prominences. Although there exist vertical flows with LOS components reaching up to 10 km s^{-1} (Peter, 1999; Hassler et al., 1999; Dammasch et al., 1999; Peter & Judge, 1999), their effect on the radiation in higher Lyman lines is quite negligible, as we will show below.

To solve the NLTE transfer problem for such a model of the coronal plasma, we use here the fast so-called MALI (Multilevel Accelerated Lambda Iterations) code originally developed for solar prominences (Heinzel, 1995). This code solves consistently the radiative transfer equations and the equations of statistical equilibrium. At the low densities considered here, the plasma volume is optically thin even in the Lyα line, and thus only a small number of numerical iterations is required by the MALI code to get convergence of the solution. We take into account 12 hydrogen atomic levels plus continuum, an approach which describes the three lines Ly6, Ly7 and Ly9 well (we did not study Ly8 because of line blends). Altogether, we deal with 78 atomic transitions for which the radiative and collisional rates are computed. We assume statistical equilibrium and that all three plasma components, i.e., the protons, electrons and hydrogen atoms, have the same kinetic temperature, and that the electron density is fully determined by hydrogen ionization. For further details about this NLTE method see, e.g., Heinzel et al. (1997), where a specific version of the MALI code was used for solar filaments.

In Table 3 we present the results of our NLTE computations for eight models which cover a reasonable range of temperatures and electron densities. The turbulent velocity, ξ, was for all models set to 20 km s^{-1}, which is a typical value for the transition region (e.g., Mariska, 1992; Chae et al., 1998). These temperatures and turbulent speed are consistent with those in Table 2, which are derived directly from the observed line widths. Electron densities in a polar coronal hole have been discussed by Wilhelm (1997); see his Fig. 17 which indicates densities around 10^8 cm^{-3} just above the limb. The parameter d_M is the geometrical LOS extension of the whole emitting volume. Its value can vary significantly depending on the real size of the plasma volume and its filamentation (filling factor). As an upper limit we can probably take a value comparable to the solar radius ($R_\odot = 6.96\ 10^5$ km). For all these parameters we show in Table 3 the line-centre model intensity, I_M, for the Ly6 line. Assuming further that the plasma is optically thin in this

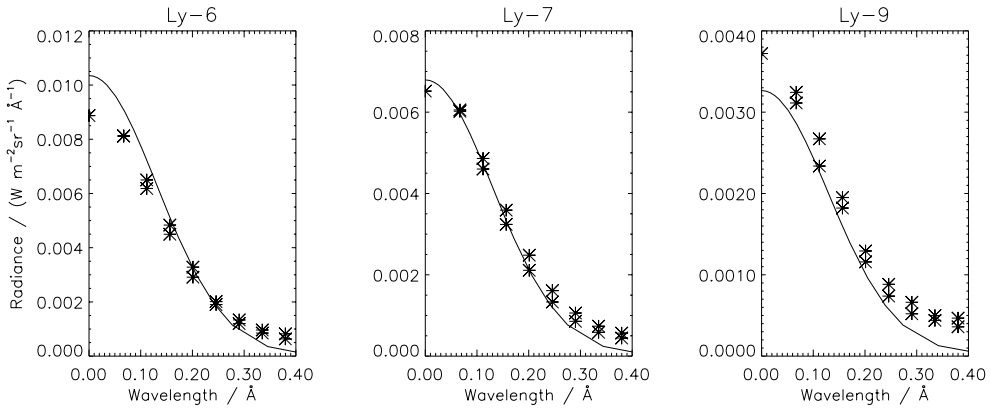

Fig. 9. Model line profiles of the spectral radiance of the H I Ly6, Ly7 and Ly9 lines in comparison with the observed line profiles as shown in the frames (b) of Figs. 6, 7, 8. Note that only half of the theoretical line profile is shown, since these profiles are symmetric. The asterisks indicate the results obtained from the observations (data set 1). The model temperature is $T = 1.2\ 10^5$ K, and the turbulence amplitude $\xi = 40$ km s^{-1}, parameters by which the observed line shapes are fitted best.

Table 3. NLTE-model parameters of the Ly6 line for eight models

	T (10^5 K)	n_e (10^8 cm^{-3})	d_M 10^6 km	I_M (line centre) (W m^{-2} sr^{-1} Å^{-1})	d_O (set 1) 10^6 km	d_O (set 2) 10^6 km
1	1.0	1.0	0.5	0.0084	0.54	0.92
2	1.5	0.8	5.0	0.0285	1.58	2.72
3	1.5	1.0	0.5	0.0044	0.10	0.18
4	1.5	2.0	0.1	0.0035	0.26	0.44
5	1.5	5.0	0.1	0.0212	0.04	0.07
6	2.0	1.0	0.5	0.0028	1.61	2.77
7	2.0	2.0	0.5	0.0110	0.41	0.70
8	2.0	5.0	0.1	0.0138	0.07	0.11

line (which is confirmed by the computations), we can obtain an "observed" LOS length, d_O, by relating I_M to the observed value of I_O, which is $I_O = 0.009$ W m^{-2} sr^{-1} Å^{-1} for data set 1 and $I_O = 0.0155$ W m^{-2} sr^{-1} Å^{-1} for data set 2. Then $d_O = d_M I_O / I_M$. Some of the models give unrealistic LOS lengths, namely models 2, 5, and 6. On the other hand, the model 4 seems to be realistic, and thus we have started with it to fit all of the three lines. By a trial-and-error method we have tried to get a best fit for the Ly6, Ly7 and Ly9 lines. Our results are shown in Fig. 9. In order to match the line widths and the central intensities, we have finally used $T = 1.2\ 10^5$ K and $\xi = 40$ km s^{-1}, which is a value larger than typical but still subsonic.

A comparison with SUMER data - the asterisks show the observed intensities in both line wings, while the model profiles are symmetrical - leads to a maximum difference of about 15% in the line core, a result which is very encouraging. The agreement becomes even better if the instrumental line broadening is corrected for, which reduces the line widths somewhat and the flanks as well. As far as the uniqueness of this model is concerned, we cannot make definite conclusions but reasonably constrain the calculations. When the range of temperatures and turbulent velocities is fixed by the observed line widths (Table 2), we are left with only two free parameters, the electron density and the thickness of the plasma column. Varying these parameters, e.g. increasing n_e and decreasing d_M, still gives rise to similar line intensities. However, we consider the electron density in model 5 as a realistic upper limit, consistent with values obtained from density-sensitive line ratios (Wilhelm, 1997; Wilhelm et al., 1998a).

Note finally, that the model used in Fig. 9 leads to an optical thickness for the Lyα line of about 0.5, and thus all higher Lyman lines are certainly optically thin. While the Lyα line is excited mainly by the incident solar radiation (this line is known to be formed by the resonance scattering of disk radiation, which also depends on the flow velocities - the so-called Doppler dimming effect; see Hyder & Lites, 1970, and Kohl et al., 1987), we find that the higher Lyman lines are quite insensitive to any incident radiation. Their emissivity is collisionally controlled by local plasma conditions (mainly by the temperature and density). However, because of the strong spontaneous radiative deexcitation, the excitation balance is far from LTE. Under such conditions, a complex NLTE approach as used in this study is required.

5. Summary and conclusions

The SUMER Spectrometer on SOHO has been used to observe the lines of the Lyman series of hydrogen emitted in the solar polar corona. Height profiles from the limb to about 70″ of the shapes and intensities of the H I Ly6, Ly7 and Ly9 lines were obtained. The lines show the typical self-absorption reversal near the limb, change systematically with increasing height and attain a Gaussian shape at relative heights between 19″ and 22″. The line shapes and intensities can be fitted well by model profiles obtained from multilevel NLTE radiative-transfer calculations, by means of which the electron density and the temperatures

of the protons and hydrogen atoms can be consistently determined. The derived temperatures range between 1 10^5 K and 2 10^5 K. Such values are also obtained if the emission is interpreted as coming from optically thin material in the lower corona, in which case the temperature and turbulence broadening can be directly obtained from fitting the emission lines by Gaussians. Yet, only the model calculations give us in addition the electron density. The model values, ranging from (1 to 2) 10^8 cm^{-3}, are in good agreement with measurements made with the line-ratio technique at similar heights in the solar atmosphere (see Wilhelm et al., 1998a). The turbulence contribution, ξ, to the line broadenings is found to range between 20 km s^{-1} and 40 km s^{-1}, amplitudes that are consistent with other estimates (Marsch et al., 1997; Tu et al., 1998; Wilhelm et al., 1998a) obtained for the lower coronal holes from heavy-ion extreme ultraviolet lines forming around $T = 10^5$ K. The values of the turbulence amplitude cited above are sufficient, according to the models of Tu & Marsch (1997) and Marsch & Tu (1997a,b), to accelerate the wind to the high terminal speeds between 600 and 800 km s^{-1} which were observed in situ over the solar poles by the Ulysses spacecraft.

The parameters derived here provide important input for models of coronal holes and solar wind acceleration (for a recent review see, e.g., Marsch 1997). In the models the asymptotic flow speed of a wind, which is driven by the gradient force of the low-frequency Alfvén-wave pressure and/or the thermal pressure generated by high-frequency Alfvén-wave heating, depends strongly on the wave-amplitude at the coronal base. Therefore, Olsen et al. (1994) suggested to study the Lyα line, particularly in order to probe the turbulence state near the coronal base. They analyzed in detail a proton-electron corona, with neutral hydrogen included as test particles, and calculated the line shape originating from scattered light as a function of height between 2 and 10 $R_\odot$. They obtained a characteristic altitude variation in the Lyα profiles, which partly resemble the ones we found for the higher Lyman lines in this study. The Lyα width is mainly determined by the Alfvén-wave-induced motion of H I perpendicular to the solar magnetic field. Similar fluid calculations still need to be carried out for the low heights (smaller than 1.06 $R_\odot$) considered in this paper.

Whereas our results are consistent with protons and electrons having still the same temperature enforced by collisional energy exchange, it is clear that all other ions heavier than α particles must be much hotter than the protons at the same height. Tu et al. (1998, 1999) presented heavy-ion temperatures as measured in a polar coronal hole in the distance range from $17''$ to $64''$ relative to the height where the N IV ($\lambda765$) line emission maximizes. They analyzed several lines of multiply-charged ions, which in LTE would form around 1 10^6 K, and found kinetic temperatures from about 2.5 to 5.0 10^6 K, and values of the related turbulence amplitude, ξ, between 20 and 40 km s^{-1}, similar to the ones derived here for H I or protons being at about 0.1 10^6 K. Although these results were obtained for different observational periods and coronal locations, its seems fair to conclude that heavy ions and protons are not in temperature equilibrium at the coronal base.

Acknowledgements. The SUMER project is financially supported by DLR, CNES, NASA, and the ESA PRODEX Programme (Swiss contribution). SUMER is part of SOHO, the Solar and Heliospheric Observatory, of ESA and NASA. Part of C.-Y.Tu's work was supported by the University of Peking, Beijing, China, and the Chinese National Natural Science Foundation. P. Heinzel acknowledges the support of MPAE during his stay in Lindau. His work was also supported by the grant No. A3003902 of the GA-AUČR.

References

Brekke P., Hassler D.M., Wilhelm K., 1997, Solar Phys. 175, 349
Carlsson M., Judge P.G., Wilhelm K., 1997, ApJ 486, L63
Chae J., Yun H.S., Poland A.I., 1998, ApJS 114, 151
Cranmer S.R., Kohl J.L., Noci, G., et al., 1999a, ApJ 511, 481
Cranmer S.R., Field G.B., Kohl J.L, 1999b, ApJ Letters, in press
Curdt W., Feldmann U., Laming J.M., et al., 1997a, A&AS 126, 281
Curdt W., Kucera A., Rybak J., Schühle U., Wöhl H., 1997b, Fifth SOHO Workshop, Oslo, Norway, ESA SP-404, 307
Curdt W., Heinzel P., 1998, ApJ 503, L95
Dammasch I.D., Wilhelm K., Curdt W., Hassler D.M., 1999, A&A, in press
David C., Gabriel A.H., Bely-Dubau F., et al., 1998, A&A 336, L90
Gabriel A.H., 1976, Phil. Trans. R. Soc. London 281, 339
Hackenberg P., Mann G., Marsch E., 1999, Space Sci. Rev., in press
Hassler D.M., Wilhelm K., Lemaire P., Schühle U., 1997, Solar Phys. 175, 375
Hassler D.M., Dammasch I.D., Lemaire P., et al., 1999, Sci 283, 810
Heinzel P., 1995, A&A 299, 563
Heinzel P., Schmieder B., Vial J.-C., 1997, Fifth SOHO Workshop, Oslo, Norway, ESA SP-404, 427
Hyder C.L., Lites B.W., 1970, Solar Phys. 14, 147
Kohl J.L., Noci G., Antonucci E., et al., 1997 Solar Phys. 175, 613
Kohl J.L., Noci G., Antonucci E., et al., 1998, ApJ 501, L127
Koutchmy S., Loucif M.L., 1991, In: Ulmschneider P., Priest E.R., Rosner R. (eds.) Mechanisms of Chromospheric and Coronal Heating. Springer, Heidelberg, Germany, p. 152
Lemaire P., Wilhelm K., Curdt W., et al., 1997, Solar Phys. 170, 105
Mariska J.T., 1992, The Solar Transition Region. Cambridge University Press, Cambridge, UK
Marsch E., 1997, 31st ESLAB Symposium, ESA-SP 415, 7
Marsch E., Tu C.-Y., 1997a, Solar Phys. 176, 87
Marsch E., Tu C.-Y., 1997b, A&A, 319, L17
Marsch E., Tu C.-Y., Wilhelm K., et al., 1997, ESA SP-404, 555
Olsen E.L., Leer E., Holzer T.E., 1994, ApJ 420, 913
Peter H., 1999, ApJ, in press
Peter H., Judge P.G., 1999, ApJ, in press
Roberts W.O., 1945, ApJ 101, 136
Seely J.F., Feldman U., Schühle U., et al., 1998, ApJ 484, L87
Tu C.Y., Marsch E., 1997, Solar Phys. 109, 149
Tu C.Y., Marsch E., Wilhelm K., Curdt W., 1998, ApJ 503, 475
Tu C.Y., Marsch E., Wilhelm K., 1999, Space Sci. Rev., in press
Warren H.P., Mariska J.T., Wilhelm K., 1998, ApJS 119, 105
Wilhelm K., Curdt W., Marsch E., et al., 1995, Solar Phys. 162, 189
Wilhelm K., 1997, Fifth SOHO Workshop, Oslo, Norway, ESA SP-404, 17
Wilhelm K., Lemaire P., Curdt W., et al., 1997a, Solar Phys. 170, 75
Wilhelm K., Lemaire P., Feldman U., et al., 1997b, Appl. Opt. 36, 6416
Wilhelm K., Marsch E., Dwivedi B.N., et al., 1998a, ApJ 503, 1023
Wilhelm K., Lemaire P., Dammasch I.E., et al., 1998b, A&A 334, 685
Vernazza J.E., Avrett E.H., Loeser R., 1973, ApJ 184, 605
Vernazza J.E., Avrett E.H., Loeser R., 1981, ApJS 45, 635